Boundary-Layer Meteorol (2006) 121:283–311
DOI 10.1007/s10546-006-9072-6

ORIGINAL PAPER

Large-eddy simulation of the dispersion of solid particles in a turbulent boundary layer

Ivana Vinkovic · Cesar Aguirre · Michel Ayrault · Serge Simoëns

Received: 29 September 2005 / Accepted: 14 March 2006 /
Published online: 3 June 2006

Abstract A large-eddy simulation (LES) with the dynamic Smagorinsky-Germano subgrid-scale (SGS) model is used to study the dispersion of solid particles in a turbulent boundary layer. Solid particles are tracked in a Lagrangian way. The instantaneous velocity of the surrounding fluid is considered to have a large-scale part (directly computed by the LES) and a small-scale part. The SGS velocity of the surrounding fluid is given by a three-dimensional Langevin model written in terms of SGS statistics at a mesh level. An appropriate Lagrangian correlation time scale is considered in order to include the influences of gravity and inertia of the solid particle. Inter-particle collisions and the influence of particles on the mean flow are also taken into account. The results of the LES are compared with the wind-tunnel experiments of Nalpanis et al. (1993 J Fluid Mech **251**: 661–685) and of Tanière et al. (1997 Exp in Fluids **23**:463–471) on sand particles in saltation and in modified saltation, respectively.

Keywords Dispersion · Large-eddy simulation · Saltation · Sand particles · Two-phase flow

1 Introduction

Sand drift by saltation and the transport of dust in suspension are the predominant manifestations of wind erosion. During an erosion event, saltation (the hopping motion of sand particles) can move large quantities of soil across the landscape over distances from metres to kilometres, causing topographic deformations such as sand dunes or soil abrasion. In this process, the soil is left without its finer constituents. These small particles become suspended in the air as dust, and can then be dispersed away from the surface by atmospheric turbulence and ultimately transported over

I. Vinkovic (✉) · C. Aguirre · M. Ayrault · S. Simoëns
LMFA, UMR CNRS 5509, Ecole Centrale de Lyon, Université de Lyon I, INSA Lyon,
69131 Ecully Cedex, France
e-mail: ivana.vinkovic@ec-lyon.fr

very large distances, up to thousands of kilometers by atmospheric circulation. Dust particles are the basic constituents of sand storms, and may be a great source of air pollution. Since the small soil particles are rich in nutrients and organic matter, dust entrainment during wind erosion leads to long-term soil degradation that is essentially irreversible.

The motion of saltation of sand particles across an erodible surface not only transports sand and similar materials but can also initiate through bombardment of the surface the entrainment and subsequent transport of other particles (Shao 2000). Therefore, an important aspect of all studies of wind erosion is the assessment of solid particle dispersion by atmospheric turbulence as well as the grain-bed interaction, also called the splash process.

Research on the transport of sediment by wind started with the classic work of Bagnold (1941), followed by the steady state theory of Owen (1964). The classical perception of the process served as a basis for many new developments, and it has been modified and sharpened at important points in recent years (e.g., Doorschot and Lehning 2002; Shao 2000, 2005). Since Bagnold (1941), research on saltation has concentrated on finding a description of the physical processes of aerodynamic entrainment, rebound, ejection and particle-wind feedback. Several numerical models for the saltation process have been developed: see Anderson and Haff (1991), McEwan and Willetts (1991) and Shao and Li (1991). Because of the model complexities, solutions are mostly found through numerical integrations, though Sorensen (1991) proposed an analytical approximation. Particles in suspension were treated with a global approach. Models determining global vertical and horizontal mass fluxes were developed mostly by Shao et al. (1996), Shao and Leslie (1997), Marticorena and Bergametti (1995), and Marticorena et al. (1997).

Since the pioneering work of Deardorff (1970), large-eddy simulation (LES) has become a well established tool for the study of turbulent flows (Meneveau and Katz 2000) as well as the transport of solid particles in a variety of conditions (Wang and Squires 1996; Shao and Li 1999). However, since only the motion of the large scales is computed, the effect of the small scales on particle dispersion, motion or deposition must be either modelled separately or neglected.

In this study, a modified Lagrangian stochastic model is coupled with a LES with the dynamic Smagorinsky-Germano subgrid-scale (SGS) model (Germano et al. 1991) in order to take into account the SGS motion of particles. The SGS velocity of solid particles is given by a modified three-dimensional Langevin model, which is written in terms of the local SGS characteristics. This way, the Lagrangian stochastic model is given by the quantities directly computed by the LES with the dynamic Smagorinsky-Germano SGS model (Germano et al. 1991) and the subgrid turbulent kinetic energy. A modified Lagrangian correlation time scale is considered in order to include the influences of gravity and inertia of the solid particle. Inter-particle collisions, grain-bed interactions (rebound, ejection, aerodynamic entrainment) and two-way coupling (particle-wind feedback) are also introduced. Knowing the SGS velocity and displacement of solid particles is important when it comes to studying inter-particle or grain-bed interactions, which in some conditions may be crucial processes in atmospheric sand dispersion.

The results of our computations are compared with the wind-tunnel experiments of Nalpanis et al. (1993) and of Tanière et al. (1997) on sand particles in saltation and modified saltation, respectively.

2 Large-eddy simulation

A turbulent boundary-layer flow is computed using the LES code ARPS 4.5.2. (Xue et al. 2000; 2001). ARPS is a three-dimensional, non-hydrostatic code where the fully compressible equations are solved with a time splitting procedure (Klemp and Wilhelmson 1978). The continuity and momentum equations obtained by grid filtering the Navier-Stokes equations are:

$$\frac{\partial \tilde{u}_i}{\partial x_i} = 0 \tag{1a}$$

$$\frac{\partial \tilde{u}_i}{\partial t} + \tilde{u}_j \frac{\partial \tilde{u}_i}{\partial x_j} = -\frac{1}{\rho_f}\frac{\partial \tilde{p}}{\partial x_i} + \frac{\partial}{\partial x_j}\left(\nu\left(\frac{\partial \tilde{u}_i}{\partial x_j} + \frac{\partial \tilde{u}_j}{\partial x_i}\right) - \tau_{ij}^r\right) + \tilde{B}_i + \tilde{f}_i\,, \tag{1b}$$

where u_i is the fluid velocity, p is the total pressure, ν the molecular kinematic viscosity, ρ_f the density and $i = 1, 2, 3$ refers to the x (streamwise), y (spanwise), and z (normal) directions respectively. $\tilde{B}_i$ includes the gravity and the Coriolis force. $\tilde{f}_i$ is an additional drag force resulting from the presence of particles, described in Sect. 6. The tilde denotes application of the grid-filtering operation. The filter width $\tilde{\Delta}$ is defined as $\tilde{\Delta} = (\Delta x \Delta y \Delta z)^{1/3}$, where Δx, Δy, Δz are the grid spacings in the x, y and z directions, respectively.

The effect of the subgrid scales on the resolved eddies in Eq. (1b) is presented by the SGS stress, $\tau_{ij}^r = \widetilde{u_i u_j} - \tilde{u}_i \tilde{u}_j$.

The pressure equation is obtained by taking the material derivative of the equation of state and replacing the time derivative of density by the velocity divergence using the mass continuity equation:

$$\frac{\partial \widetilde{\Delta p}}{\partial t} + \tilde{u}_j \frac{\partial \widetilde{\Delta p}}{\partial x_j} = \frac{\rho_f}{c^2}\left(\frac{1}{\tilde{\theta}}\frac{\partial \tilde{\theta}}{\partial t} - \frac{\partial \tilde{u}_i}{\partial x_i}\right), \tag{2}$$

where Δp is the pressure deviation from an undisturbed dry, hydrostatic base state, c is the speed of sound and θ the potential temperature. The flow studied here is a neutral turbulent boundary layer, so that the potential temperature variations are therefore negligible. By avoiding the resolution of the Poisson equation for pressure, in compressible models such as ARPS (Xue et al. 2000) or MM5 (Dudhia 1993), all computations are local to the grid points involved in the finite difference stencil, making their implementation on distributed-memory parallel processor computers straightforward through the use of domain decomposition strategies (Johnson et al. 1994). Different from anelastic systems (Lafore et al. 1998), the compressible system of equations does not have to make any approximation, making it suitable to a wider range of applications.

The determination of the SGS stress, τ_{ij}^r, is parameterized using an eddy viscosity hypothesis:

$$\tau_{ij}^r - \tfrac{1}{3}\delta_{ij}\tau_{kk}^r = -2K_m\tilde{S}_{ij}, \tag{3}$$

where the turbulent eddy viscosity K_m is:

$$K_m = C\tilde{\Delta}^2|\tilde{S}|, \tag{4}$$

the resolved-scale strain tensor is defined as

$$\tilde{S}_{ij} = \frac{1}{2}\left(\frac{\partial \tilde{u}_i}{\partial x_j} + \frac{\partial \tilde{u}_j}{\partial x_i}\right), \tag{5}$$

and $|\tilde{S}| = \sqrt{2\tilde{S}_{ij}\tilde{S}_{ij}}$ is the magnitude of $\tilde{S}_{ij}$. The model coefficient C in Eq. (4) is determined locally and instantaneously with the dynamic SGS closure developed by Germano et al. (1991) and modified by Lilly (1992).

The dimensions of the computational domain in the streamwise, spanwise and wall-normal directions are, respectively, $l_x = 30H$, $l_y = 6H$ and $l_z = 2H, H$ being the boundary-layer depth. The grid is uniform in the xy planes and stretched in the z-direction by a hyperbolic tangent function.

The rigid ground boundary condition is applied at the wall. On the top of the domain and in the spanwise direction the mirror free-slip and the periodic boundary conditions are applied, respectively. In the streamwise direction, at the end of the domain, the wave-radiation open boundary condition is used (Klemp and Wilhelmson 1978) in order to allow waves in the interior of the domain to pass out freely through the boundary with minimal reflection. At the beginning of the domain, in the streamwise direction, forcing is applied. The dataset is obtained from the experimental results of Fackrell and Robins (1982).

3 The motion of solid particles

For particles with a density much greater than the density of the carrier fluid $\left(\rho_p/\rho_f \geq 10^3\right)$, and with a diameter d_p smaller than the Kolmogorov scale, a simplified equation of motion including only the drag and gravity forces can be considered:

$$\frac{d\vec{x}_p(t)}{dt} = \vec{v}_p(t) \tag{6a}$$

$$\frac{d\vec{v}_p(t)}{dt} = \frac{\vec{v}\left(\vec{x}_p(t), t\right) - \vec{v}_p(t)}{\tau_p} f\left(Re_p\right) + \vec{g}, \tag{6b}$$

where $\vec{v}_p$ is the velocity of the particle, $\vec{v}\left(\vec{x}_p(t), t\right)$ is the velocity of the fluid at the particle position and $\vec{g}$ is the acceleration of gravity. The particle relaxation time is given by:

$$\tau_p = \frac{\rho_p d_p^2}{18\rho_f \nu}, \tag{7}$$

and

$$Re_p = \frac{|\vec{v}_p - \vec{v}|d}{\nu}, \tag{8}$$

is the particle Reynolds number. Effects of nonlinear drag are incorporated through $f\left(Re_p\right)$ and in this work an empirical relation from Clift et al. (1978) is used:

$$f\left(Re_p\right) = 1 \quad \text{if} \quad Re_p < 1, \tag{9a}$$

$$f\left(Re_p\right) = 1 + 0.15Re_p^{0.687} \quad \text{if} \quad Re_p \geq 1. \tag{9b}$$

Eq. (6b) is appropriate for describing the motion of smooth rigid spheres, and neglects the influence of all the other forces such as the virtual mass or the Basset history force, for example. The driving fluid velocity $\vec{v}\left(\vec{x}_p(t), t\right)$ is given by the velocity field of the

LES and a fluctuating subgrid component determined by a modified Lagrangian stochastic model (Sect. 4.2).

The global behaviour of particles in a turbulent flow can be characterized by the Stokes number and the gravity parameter also called the crossing trajectory parameter (Tanière et al. 1997). The Stokes number is mainly a measure of the inertia effect, and characterizes the ability of the particle to follow the fluid flow. It can be defined as the ratio of the particle relaxation time τ_p to the Lagrangian correlation time scale T_L:

$$St_L = \frac{\tau_p}{T_L}\,, \tag{10}$$

or to the Kolmogorov time scale τ_η:

$$St_\eta = \frac{\tau_p}{\tau_\eta}\,. \tag{11}$$

The Lagrangian correlation time scale T_L may be considered as proportional to the large-eddy turnover time. In this study, the time scales T_L and τ_η are estimated by:

$$\tau_\eta \sim \sqrt{\frac{\nu H}{(0.1U_e)^3}} \tag{12a}$$

and

$$T_L \sim \frac{H}{0.1U_e}\,, \tag{12b}$$

where U_e is the external velocity.

If $St_\eta << 1$, the velocity fluctuations of the particle are nearly the same as those of the fluid, and particles follow quite well the fluid flow. This behaviour is called 'pure suspension' (Tanière et al. 1997). If $St_L >> 1$, the motion of particles is not influenced by turbulence and it is mainly governed by gravity and inertia (deterministic trajectories) and collisions with the solid boundaries (Tanière et al. 1997) This behaviour is called 'pure saltation'. Between these two cases, when the relaxation time of the particle is of the same order of magnitude as the fluid time scales T_L or τ_η, we may expect some intermediate behaviour. In such conditions, both gravity and inertia, act on the particle and the gravitational parameter:

$$\gamma = \frac{v_g}{\sigma_3}\,, \tag{13}$$

is used to classify the behaviour of particles. $v_g = g\tau_p$ represents the settling velocity, and σ_3 is the vertical fluid root-mean-square velocity.

If $\gamma < 1$ we define a 'modified suspension' transport mode and if $\gamma > 1$ particles are in 'modified saltation'.

4 Stochastic model for the SGS motion of solid particles

4.1 Fluid particles

The SGS velocity of solid particles is given by analogy with the SGS stochastic model for fluid particle dispersion (Vinkovic et al. 2005a). Namely, the Lagrangian velocity of the fluid particle is given by:

$$v_i(t) = \tilde{u}_i(\vec{x}(t)) + v_i'(t) \,. \tag{14}$$

This velocity is considered to have an Eulerian large-scale part $\tilde{u}_i(\vec{x}(t))$ (which is known) and a fluctuating SGS contribution $v_i'(t)$, which is not known and will be modelled by the stochastic approach. The movement of fluid elements at a subgrid level is given by a three-dimensional Langevin model:

$$dv_i = \left(\gamma_i + \alpha_{ij}\left(v_j - \tilde{u}_j(\vec{x}_p, t)\right)\right)dt + \beta_{ij}d\eta_j(t) \,, \tag{15a}$$

$$dx_i = v_i dt \,, \tag{15b}$$

where $d\eta_j$ is the increment of a vector-valued Wiener process with zero mean $\langle d\eta_j \rangle = 0$, and variance dt, $\langle d\eta_i d\eta_j \rangle = dt\delta_{ij}$. The fluid particle velocity is given by a deterministic part $\gamma_i + \alpha_{ij}v_j'$ and by a completely random part $\beta_{ij}d\eta_j$. The coefficients α_{ij}, β_{ij} and γ_i are determined by relating the subgrid statistical moments of $\vec{v}(t)$ to the filtered Eulerian moments of the fluid velocity, in analogy with van Dop et al. (1986) who developed this approach in the case of a classic Reynolds averaged decomposition. Since we assume that the subgrid turbulence is homogeneous and isotropic (basic assumption of the LES), the total velocity of fluid elements given by the Langevin model can be written as:

$$dv_i = \left[\frac{\partial \tilde{u}_i}{\partial t} + \frac{\partial(\tilde{u}_i\tilde{u}_j)}{\partial x_j} + \frac{\partial \tau_{ij}}{\partial x_j} + \frac{3}{2}\frac{v_i - \tilde{u}_i}{\tilde{k}}\left(\frac{1}{3}\frac{d\tilde{k}}{dt} - \frac{C_0\tilde{\varepsilon}}{2}\right)\right]dt + \sqrt{C_0\tilde{\varepsilon}}\,d\eta_i(t) \,, \tag{16}$$

where $\tilde{k}$ is the subgrid turbulent kinetic energy, $\tilde{\varepsilon}$ is the subgrid turbulent dissipation rate and C_0 is the Lagrangian constant. Each fluid particle has a large-scale and a subgrid-scale velocity component. The large-scale velocity of the fluid particle is directly computed by the LES, and the subgrid-scale velocity component is obtained from the dynamic Smagorinsky-Germano SGS model. An additional transport equation for $\tilde{k}$ is resolved, and is deduced from Deardorff (1980):

$$\frac{\partial \tilde{k}}{\partial t} + \tilde{u}_j\frac{\partial \tilde{k}}{\partial x_j} = \frac{K_m}{3}\frac{g}{\theta_0}\frac{\partial \tilde{\theta}}{\partial z} + 2K_m\tilde{S}_{ij}^2 + 2\frac{\partial}{\partial x_j}\left(K_m\frac{\partial \tilde{k}}{\partial x_j}\right) + \tilde{\varepsilon} + \widetilde{u_i'f_i'} \tag{17}$$

where $\tilde{\varepsilon} = C_\varepsilon\tilde{k}^{3/2}/\tilde{\Delta}$ and u_i' is the SGS velocity in the LES. The terms on the right-hand-side of Eq. (17) correspond to the production by buoyancy, the production by shear, the diffusion of $\tilde{k}$, the dissipation and the additional term due to the presence of particles (described in Sect. 6). Since we are interested in neutral flows the potential temperature variation is neglected. The turbulent eddy viscosity K_m is computed by a dynamic procedure as described in the previous section.

By substracting the large-scale velocity increments on both sides of Eq. (16), the following stochastic differential equation governing the subgrid-scale fluid particle velocity, dv_i' is obtained:

$$dv_i' = \left(-\frac{1}{T_L} + \frac{1}{2\tilde{k}}\frac{d\tilde{k}}{dt}\right)v_i'dt + \sqrt{\frac{4\tilde{k}}{3T_L}}\,d\eta_i(t) \,, \tag{18}$$

where T_L is the Lagrangian correlation time scale, given by:

$$T_L = \frac{4\tilde{k}}{3C_0\tilde{\varepsilon}} \,. \tag{19}$$

The coupling between the LES and the subgrid stochastic model for fluid particles has been validated in comparison with experimental results on passive scalar dispersion in a turbulent boundary layer. Details of the validation can be found in Vinkovic et al. (2005b), and will not be presented here.

4.2 Solid particles

There are two possible Lagrangian stochastic approaches to the calculation of heavy particle trajectories. The first is to formulate the Lagrangian stochastic model directly in terms of heavy-particle velocity statistics and time scales (Reynolds 1999). The key difficulty with this approach is to deduce heavy particle velocity statistics and time scales from the specified Eulerian fluid statistics. The second approach is to calculate particle velocities directly from the particle equation of motion using simulated fluid velocities at the heavy particle position (Reynolds 2000). The central difficulty with this approach lies in the determination of the fluid velocity along the heavy particle trajectory. This velocity is neither Eulerian nor fluid Lagrangian, since both the position of the heavy particle and the fluid element occupying that position are changing. Nevertheless, these models remain consistent with prescribed Eulerian fluid velocity statistics when the particles have finite inertia and finite settling velocity and predict particle-velocity statistics, particle deposition velocities and mean particle concentrations in close agreement with experimental or direct numerical simulation data (Reynolds 2000).

Because of their inertia effects and their different responses to gravity, solid particles deviate from the fluid element that originally contained them, inducing a decorrelation. The main difficulty lies in the determination of the fluid particle velocity along the solid particle trajectory, $\vec{v}\left(\vec{x}_p(t),t\right)$. This fluid velocity is computed with Eq. (14) and by analogy with Eq. (18) where T_L is replaced by T_L^p, a Lagrangian decorrelation time scale of the fluid velocity along the solid particle trajectory. In order to account for gravity and inertia effects, we expect the modified time scale to be shorter than the fluid Lagrangian time scale T_L. The velocities to which a solid particle is subjected will not be as well correlated as those to which a fluid particles is subjected. Moreover, as noted by Rodgers and Eaton (1990), a frequency measured in a Lagrangian frame is always lower than a frequency measured in an Eulerian one. Different forms have been previously developed for T_L^p, see Sawford and Guest (1991) and Zhuang et al. (1989), for example. We propose the following formulation:

$$T_L^p = \frac{T_L}{\alpha_{\text{grav}} + \alpha_{\text{inert}}}\,, \tag{20}$$

where α_{grav} and α_{inert} are the coefficients relative to gravity and inertia effects. Details of this formulation may be found in Aguirre et al. (2004), and we will give here only the main ideas.

The gravity effect is estimated following the approximation of Csanady (1963), who proposed an interpolation between the Lagrangian correlation for vanishing inertia and small terminal velocity v_g, and the Eulerian correlation for large v_g. In the direction parallel to gravity, α_{grav} is given by:

$$\alpha_{\text{grav}} = \sqrt{1 + \left(\frac{\beta v_g}{\tilde{\sigma}}\right)^2}\,, \tag{21}$$

where $\tilde{\sigma} = \sqrt{2\tilde{k}/3}$ and β is the ratio of Lagrangian to Eulerian time scales $\beta = T_L/T_E$. For SGS velocity fields we assume $\beta = 1$ (Pozorski et al. 2004; Yeung 2001; Hanna 1981).

Following the ideas of Csanady (1963), Wang and Stock (1993) introduced the inertia effects by considering instead of T_L, an integral time scale T that is a function of particle inertia. This time scale, T, has been obtained from numerical simulations. Pozorski and Minier (1998) developed a stochastic model by considering separately the effects of inertia and gravity. The modified integral time scale, proposed by Pozorski and Minier (1998), is given by the Lagrangian and Eulerian fluid time scales and the ratio of the solid particle velocity variance to the fluid velocity variance, $x = \sigma_p/\sigma_f$. At each timestep, this modified integral time scale takes into account the instantaneous relative velocity between the solid and the fluid particle.

In this study, the inertia effect is evaluated in the case of large inertia and vanishing v_g. A turbulent structure (length scale l) passing by a the moving particle would have a frequency of:

$$\nu_{\text{part}} = \frac{\left|\vec{v}\left(\vec{x}_p(t),t\right) - (\vec{v}_p - \vec{v}_g)\right|}{\tilde{\sigma}} \nu_L = \alpha_{\text{inert}} \nu_L \,, \tag{22}$$

where ν_L represents the Lagrangian correlation time scale.

There are three limiting cases that a Lagrangian stochastic model for heavy particles should satisfy:

- In the limit of vanishing inertia ($\tau_p \to 0$) and vanishing terminal velocity ($v_g \to 0$), the particle is equivalent to a fluid element and $T_L^p \to T_L$.
- In the limit of large settling velocity ($v_g \to \infty$), the particle trajectory approaches a straight line through the fluid and the $T_L^p \to T_E^m$, T_E^m being the Eulerian space-time correlation with space separation $v_g dt$.
- In the limit of large inertia ($\tau_p \to \infty$) but small terminal velocity ($v_g \to 0$), the particle is effectively stationary over a time period T_E and we have $T_L^p \to T_E$.

The model proposed in this study satisfies the limiting cases described above.

Recently, Shao (1995) and Reynolds and Cohen (2002) have pointed out some contradictions relative to the structure function of $\vec{v}'\left(\vec{x}_p(t),t\right)$ and suggested that this velocity should be evaluated using a fractional Langevin equation. In fact, Wiener increments necessarily lead to a structure function proportional to dt when, in the limiting case of large drift velocity and negligible inertia, the driving fluid velocity correlation approaches the Eulerian space-time correlation that is proportional to $dt^{2/3}$. However, the saltating particles being far from these limiting cases, in a way identical to Reynolds (2000), we will forsake considerations of the structure function for increments in fluid velocity and treat $d\eta_j$ as increments of a Wiener process.

5 Particle collisions

The developed inter-particle collision model relies on particle pairing and the calculation of the collision probability according to the kinetic theory. This model is inspired by the inter-particle collision model of Sommerfeld (2001), where the generation of a fictitious collision partner is replaced by particle pairing.

The domain is divided into boxes that are small compared to the length scale of the flow (Pope 1985). In each box, at each timestep, solid particles are randomly selected

by pairs. For each pair (i, j) the probability for the occurrence of a collision is determined. This collision probability is calculated as the product of the timestep dt and the collision frequency given by the kinetic theory (Sommerfeld 2001):

$$dP_{\text{coll}} = f_c dt = \frac{\pi}{4} \left(d_{p,i} + d_{p,j}\right)^2 \left|\vec{v}_{p,i} - \vec{v}_{p,j}\right| n_p dt \,, \tag{23}$$

where $d_{p,i}$ and $d_{p,j}$ are the particle diameters, $\left|\vec{v}_{p,i} - \vec{v}_{p,j}\right|$ is the instantaneous relative velocity of the selected pair and n_p is the number of particles per unit volume in the respective box. In order to ensure that the collision probability is less than unity, the timestep has to be 20% of the minimum of the inter-particle collision time, given by

$$\tau_c = \frac{1}{\frac{\pi}{4}(d_{p,\max} + d_{p,\min})^2 \left|\Delta\vec{v}_{p,max}\right| n_p} \,, \tag{24}$$

where $d_{p,\max}$ and $d_{p,\min}$ represent the local maximum and minimum particle diameters and $\Delta\vec{v}_{p,\max}$ is the estimated maximum relative velocity between the particles.

In order to decide whether a collision takes place, a random number ξ from a uniform distribution in the interval $[0, 1]$ is generated. A collision occurs when the random number becomes smaller than the collision probability, i.e., if $\xi < P_{\text{coll}}$.

The relations for the calculation of the post-collision velocities of the considered particles in the co-ordinate system where one particle is stationary are given by the momentum equations for an oblique central collision. By solving the momentum equations in connection with Coulomb's law of friction and neglecting particle rotation, one obtains the following equations for the determination of the velocity components of the considered particles after collision, $(v'_{p,i,x}, v'_{p,i,z})$, the symbol prime denoting here the velocity after collision:

$$v'_{p,i,x} = v_{p,i,x}\left(1 - \frac{1+e}{1 + m_{p,i}/m_{p,j}}\right) . \tag{25}$$

For a non-sliding collision:

$$v'_{p,i,z} = v_{p,i,z}\left(1 - \frac{1/7}{1 + m_{p,i}/m_{p,j}}\right) . \tag{26}$$

For a sliding collision:

$$v'_{p,i,z} = v_{p,i,z}\left(1 - \mu(1+e)\frac{v_{p,i,x}}{v_{p,i,z}}\frac{1}{1 + m_{p,i}/m_{p,j}}\right) , \tag{27}$$

where the condition for a non-sliding collision is:

$$\frac{v_{p,i,x}}{v_{p,i,z}} < \tfrac{7}{2}\mu(1+e) \,. \tag{28}$$

Here $e = 0.95$ (Fohanno and Oesterlé 2000) is the coefficient of restitution, $\mu = 0.4$ (Fohanno and Oesterlé 2000) is the coefficient of friction, and $m_{p,i}$ and $m_{p,j}$ are the masses of the considered particles. In this model, inelasticity is taken into account by using Newton's hypothesis that assumes a constant ratio between the post- and pre-collisional velocities. This ratio defines the coefficient of restitution e. The coefficient of static friction μ determines the force necessary to stop sliding during the collision time. If the condition for a sliding collision $(v_{p,i,x}/v_{p,i,z} > (7/2)\mu(1+e))$ is satisfied a relative tangential velocity will still exist after the impact.

Tanaka and Tsuji (1991) as well as Yamamoto et al. (2001), found that the effect of inter-particle collisions on the dispersion in the direction normal to the mean flow cannot be neglected even for a volume fraction of $\Phi_p \sim 10^{-4}$.

6 Two-way coupling

The influence of the presence of particles on the fluid motion has not yet been fully understood. In some cases, e.g., bubble flow, the presence of particles may produce velocity fluctuations of the surrounding fluid whose wavelength is smaller than the particle diameter.

However, it was numerically shown by Pan and Banerjee (1996) that the particles work as if they were an extra burden to the fluid when the particles are small and have much larger density than the surrounding fluid, as is the case in the present study. In such a case, the momentum transfer from particles to fluid can be successfully modelled by adding the reaction force $\tilde{f}_i$, against the surface force acting on the particle to the Navier-Stokes equation, Eq. (1b). The additional drag force is then given by (Yamamoto et al. 2001):

$$\tilde{f}_i = -\frac{1}{\rho_f V_{grid}} \sum_{p=1}^{Np} m_p \frac{u_i\left(\vec{x}_p(t), t\right) - v_{p_i}(t)}{\tau_p} f\left(Re_p\right) \ , \tag{29}$$

where V_{grid} is the volume of the grid cell and N_p is the number of particles per grid. This model is sometimes referred to as the force coupling model in contrast to the velocity coupling model (Pan and Banerjee 1996) in which the velocity disturbance around the particle is considered.

When two-way coupling is modelled by the force coupling model, as mentioned above, an extra term appears in the transport equation of the subgrid turbulent kinetic energy, Eq. (17):

$$\widetilde{u_i' f_i'} = \frac{\rho_p \Phi_p}{\rho_f \tau_p} \left(\widetilde{u_i' v_i'}\left(\vec{x}_p(t), t\right) - \widetilde{u_i' v_{p_i}'} \right) f\left(Re_p\right) \ , \tag{30}$$

where f_i' is the fluctuation component of the force from particles to fluid, f_i, and ϕ_p is the volume fraction in the grid cell occupied by the particles. Although several formulae have been proposed for the approximation of $\widetilde{u_i' v_{p_i}'}$, the model by Porahmadi and Humphrey (1983):

$$\widetilde{u_i' v_{p_i}'}\left(\vec{x}_p(t), t\right) = \frac{2\tilde{k}}{1 + \tau_p / T_L} \ , \tag{31}$$

has been adopted for simplicity. In addition to this, we assume that $\widetilde{u_i' v_i'}\left(\vec{x}_p(t), t\right) = 2\tilde{k}$. Therefore, the additional term in the transport equation of the subgrid turbulent kinetic energy can be written as:

$$\widetilde{u_i' f_i'} = -\frac{\rho_p \Phi_p}{\rho_f} \frac{2\tilde{k}}{\tau_p + T_L} f\left(Re_p\right) \ . \tag{32}$$

In the test cases presented here, close to the wall, the volume fractions are $\Phi_p \sim 10^{-5}$ (Nalpanis et al. 1993) and $\Phi_p \sim 10^{-4}$ (Tanière et al. 1997). Classically, two-way coupling is included for $\Phi_p \geq 10^{-6}$, as claimed by Elghobashi (1994).

7 Particle-bed interactions

7.1 Rebound and ejection

Due to gravitational acceleration, all sand particles impact the ground and, if the particles are in movement over a sand bed, as they impact the surface, they interact energetically with a group of nearby particles within the bed. This mechanism of interaction called the splash process is extremely complicated, and must take into account the reaction not only of the grain impacting the ground, but the resulting rearrangements of the grains in the bed, including the possibility of ejection of new grains, and rebound of the impacting particle.

Using high-speed photographic techniques Rice et al. (1996) carried out experiments to examine the possible mechanism of dust emission by saltation. Their observations revealed that sand grains saltating over a surface of loose fine particles excavate craters in the bed. Rice et al. (1996) proposed a deterministic model that estimates the dust emission rate as the volume removed by impacting sand grains as they plough into the soil surface. For individual impacting events, Lu and Shao (1999) developed the equations of motion for the saltating grain in the bed that is deformed plastically, so that the removed volume is obtained by integrating those equations. The vertical dust flux is then obtained by multiplying the removed volume by a bulk density, the number of impacting grains and the fraction of dust contained in the soil.

Because of the complicated microtopography of even a 'flat' bed, and because of the complexity of the packing geometry, the splash process in this study is considered as stochastic. The results of any particular impact characterized by the size of the impacting grain, its angle and speed, and the nature of the local bed (grain size distribution, angle with respect to horizontal) are known only in a statistical sense. Numerous authors (e.g., White and Schulz 1977; Willetts and Rice 1986; Willetts et al. 1991; McEwan et al. 1992; Mitha et al. 1986) developed rather complete statistical descriptions of the impact process during sparse saltation in wind-tunnel settings with uniform grains. Most frequently, the inputs of the splash function are the diameter of the impacting grain, the speed and angle of approach. The impact results in two phenomena: the rebound and the ejection of several new grains from within the bed.

The statistical laws used in our approach derive mostly from the models proposed by Anderson and Haff (1991) and Sorensen (1991). Some coefficients were adapted from the experimental observations of Nalpanis et al. (1993), who measured different characteristics of sand grain trajectories by means of multiple-image photography.

The model presented here for the splash process is only based on the velocity of the impacting grain, and it is independent of the diameter of the impacting sand particle. The size distribution of the newly ejected particles is obtained from the initial size distribution of the sand bed.

As a particle impacts the sand bed, it rebounds. The norm of the velocity $|v_{reb}|$ and the angle α_{reb} after rebound are extracted from a uniform probability density with mean and standard deviation given by:

$$|v_{\mathrm{reb}}| = 0.3|v_{\mathrm{imp}}| \pm 0.25|v_{\mathrm{imp}}|\,, \tag{33a}$$

$$\alpha_{\mathrm{reb}} = 30^\circ \pm 15^\circ\,, \tag{33b}$$

$|v_{\mathrm{imp}}|$ being the norm of the impact velocity. Eq. (33a) implies that the mean and the standard deviation of the uniform probability density are $0.3|v_{\mathrm{imp}}|$ and $0.25|v_{\mathrm{imp}}|$,

respectively. Nalpanis et al. (1993) measured that, on average, the rebound velocity represents 0.5–0.6 of the impact velocity. Anderson and Haff (1991) and McEwan and Willetts (1991) obtain the same coefficient as Nalpanis et al. (1993), while Mitha et al. (1986) measured a coefficient between 0.16 and 0.2. The rebound velocity is difficult to determine, with a range in the literature of from 0.1 to 0.6. We chose $|v_{\mathrm{reb}}| = 0.3|v_{\mathrm{imp}}| \pm 0.25|v_{\mathrm{imp}}|$, which allows us to be in the limits of such a range. As for α_{reb}, the authors cited above find that on average the angle of rebound is around 30°.

If a given impact is strong enough ($|v_{\mathrm{imp}}| \geq |v_{cr}|$), new particles from the sand bed may be ejected into the flow, where v_{cr} is a critical velocity below which the impacting grain has insufficient energy to eject new grains (Sorensen 1991). Here we chose $|v_{cr}| = 0.3\ \mathrm{m\ s^{-1}}$. The initial velocity $|v_{ej}|$ and angle α_{ej} of ejected grains are extracted from a uniform probability density with mean and standard deviation given by:

$$|v_{ej}| = 0.3|v_{imp}| \pm 0.5|v_{ej}|\ , \tag{34a}$$

$$\alpha_{ej} = 60^{\circ}\ . \tag{34b}$$

Unfortunately, Nalpanis et al. (1993) could not measure the difference between rebound particles and new ejections. In their numerical simulations, Andersonn and Haff (1991) find that the ejection velocity represents 10% of the impact velocity.

The number k of newly ejected sand particles is determined according to the analytic model of Sorensen (1991), who assumed that, given the vertical component of the impact velocity $v_{3,\mathrm{imp}}$, k follows a Poisson distribution with mean value $2.9v_{3,\mathrm{imp}}$, i.e.:

$$p(k/v_{3,\mathrm{imp}}) = \frac{(2.9v_{3,\mathrm{imp}})^k e^{2.9v_{3,\mathrm{imp}}}}{k!}\ . \tag{35}$$

Therefore, the probability for ejection to happen at all depends only on the vertical component of the impacting velocity, and is given by:

$$p_{ej} = 1 - p(0/v_{3,\mathrm{imp}}) = 1 - e^{2.9v_{3,\mathrm{imp}}}\ . \tag{36}$$

The influence of different coefficients involved in the splash function on the mass flux and impact statistics was tested and is described in detail in Vinkovic (2005). For sand particles in movement over a flat bed without sand, simple symmetry conditions are applied as particles impact the wall.

7.2 Aerodynamic entrainment

The study of the particle take-off phenomenon in a turbulent boundary layer is a complicated problem, encountered in various domains concerned with fluid dynamics. The complexity arises from the fact that the motion of an individual particle results from its interaction with the near-wall turbulence, with the other particles set in motion, and with the sand bed.

Bagnold (1941) described the basis of the phenomenon and his results inspired most sediment transport models developed up to now. An exhaustive review of these models is presented in Anderson (1986). More recently, Kaftori et al. (1995) used flow visualization techniques and laser Doppler anemometry to study the motion, entrainment and deposition of solid particles near the wall in a turbulent boundary layer. They showed that particle entrainment is controlled by the action of coherent wall structures and funnel vortices. Batt et al. (1999) studied experimentally the entrainment of sand particles in a turbulent boundary layer at high friction velocities, using

measurements of dust densities and streamwise soil flux. McKenna Neuman (2003) conducted wind-tunnel experiments in order to analyze the influence of air temperature and humidity upon the threshold for particle motion. This author revised the threshold friction model of Shao and Lu (2000) to incorporate the inter-particle force associated with hygroscopic water.

In our study, the motion of sand grains is initiated by a statistical model for the aerodynamic entrainment, where the initial velocity is given as a function of the mean shear velocity u_*. The coefficients of the model are given by the experimental observations of Nalpanis et al. (1993):

$$v_{1,\text{init}} = 4u_* \pm 2u_* \,, \tag{37a}$$

$$v_{2,\text{init}} = 0 \,, \tag{37b}$$

$$v_{3,\text{init}} = 2u_* \pm u_* \,. \tag{37c}$$

The aerodynamic entrainment is only modelled here in the case of a friction velocity that is above the threshold. We therefore considered that the initial velocity of the particles is proportional to the friction velocity and that the size distribution is given by the initial size distribution measured experimentally. When applying the model to prognostic estimations a more sophisticated model should be developed, taking into account the particle size distribution and the threshold friction velocity.

White and Schulz (1977) found experimentally that the mean initial velocity for quartz particles of 350 μm in diameter is around $0.5u_*$. The numerical analysis of Shao and Li (1999) showed that, if the initial vertical velocity of sand grains is smaller than u_*, particles will be in "weak saltation". In that case the maximal saltation height attained by the particles is small and no new sand grains are ejected. If $v_{3,\text{init}}$ becomes larger than u_*, particles are in "strong saltation" and may eject new sand grains during hopping. Finally, Foucaut and Stanislas (1997) tried to determine the critical shear velocity for which sand particles are entrained by the flow. Unfortunately, they did not measure the entrainment velocity of the grains.

8 Model predictions and discussion

The LES (Sect. 2) coupled with Lagrangian particle tracking (Sect. 3), the subgrid stochastic model (Sect. 4.2), the collision model (Sect. 5), the particle-wind feedback (Sect. 6) and the splash function (Sect. 7) is validated in comparison with the wind-tunnel experiments of Nalpanis et al. (1993) and Tanière et al. (1997).

Nalpanis et al. (1993) studied the saltation of sand grains over a sand bed and, by means of multiple-image photographs, they measured ejection and impact velocities, trajectory lengths and maximum rise heights. Vertical profiles of mass flux at the end of the sand bed are determined by 12 isokinetic samplers, whose inlet speed is adjusted to the local velocity profile.

In the wind-tunnel experiment of Tanière et al. (1997), the dispersion of sand and PVC particles in a turbulent boundary layer over a flat bed without particles was studied. This case was simulated without the splash function and with simple symmetry conditions for particle rebound. This way, an additional validation without the influence of the splash model is achieved. Tanière et al. (1997) used a laser Doppler anemometry system to measure the mean and root-mean-square velocities of air and particles. Mass flux profiles were obtained by isokinetic sampling.

8.1 Saltating particles over a sand bed, Nalpanis et al. (1993)

A full description of the experimental facility and results can be found in Nalpanis et al. (1993). Here, the main characteristics of the experiment necessary for understanding the simulations are given.

A turbulent boundary layer over a sand bed is generated and downwind of the vorticity generators the floor is covered with loose sand. The main characteristics of the flow and particles are given in Table 1, noting that the size distribution of the sand particles is log-normal. Profiles of mass flux and wind speed are measured at distances 2 m, 4 m and 6 m from the upwind edge of the sand bed. Only the measurements made at 6 m are presented in Nalpanis et al. (1993).

The numerical simulation is conducted for the real wind-tunnel flow, using a grid with $156 \times 32 \times 32$ points. The grid spacing in the longitudinal and transverse direction is $\Delta x/H = \Delta y/H = 0.2$. In the vertical direction, the average grid is $\Delta z_{\text{mean}}/H = 0.1$ and the first grid point is at $\Delta z_{\text{min}}/H = 0.025$.

Figures 1 and 2 show predicted profiles of mean fluid velocity U and turbulent kinetic energy k compared to the experimental data. The turbulent kinetic energy profile is compared to the normalized profile measured by Fackrell and Robins (1982), because the corresponding profile was not published by Nalpanis et al. (1993). The mean values are obtained by averaging the fluctuating field over the horizontal extent of the domain and also over a time period sufficiently long to obtain stable statistics. The LES resulted in a fairly accurate prediction of the mean velocity.

Close to the sand bed, the volume fraction of sand particles is $\Phi_p \sim 10^{-5}$. Nevertheless, there are no noticeable effects of the two-way coupling on the mean fluid velocity profile or on the turbulent kinetic energy. The presence of particles, in this case, does not modify the properties of the carrier fluid. A numerical simulation with a higher volume fraction ($\Phi_p = 10^{-2}$) has been performed in order to check the influence of this parameter. The results of this case are presented in Vinkovic (2005).

For the turbulent kinetic energy the SGS part, the resolved part and the total of the calculated field are separated. The SGS contribution $\tilde{k}$ is obtained from Eq. (17). The LES shows discrepancies near the wall, where the fluctuations are mostly parameterized. Probably, the increasing anisotropy near the wall is not correctly represented by our correction.

Table 1 Flow and particle characteristics, Nalpanis et al. (1993)

Boundary-layer height	$H = 0.2\,\text{m}$
External velocity	$U_e = 6.3\,\text{m s}^{-1}$
Friction velocity	$u_* = 0.35\,\text{m s}^{-1}$
Roughness	$z_0 = 100 \times 10^{-6}\,\text{m}$
Mean particle diameter	$d_p = 188 \times 10^{-6}\,\text{m}$
Diameter standard deviation	$1.18 \times 10^{-6}\,\text{m}$
Particle density	$\rho_p = 2650\,\text{kg m}^{-3}$
Stokes number	$St_L = 0.97$
	$St_\eta = 88.6$
Gravity parameter	$\gamma = 5.9$
Volume fraction	$\Phi_p \sim 10^{-5}$

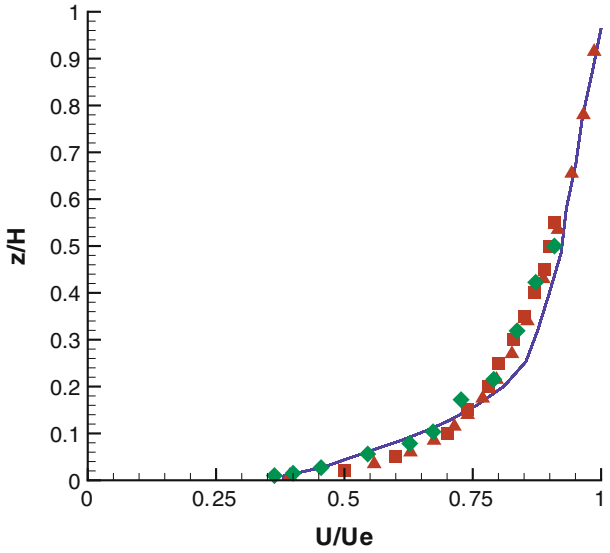

Fig. 1 Vertical profile of streamwise mean fluid velocity. Continuous line — our simulation; squares—Fackrell and Robins (1982); triangles—log law $ku/u_* = \log(z/z_0)$; diamonds—Nalpanis et al. (1993)

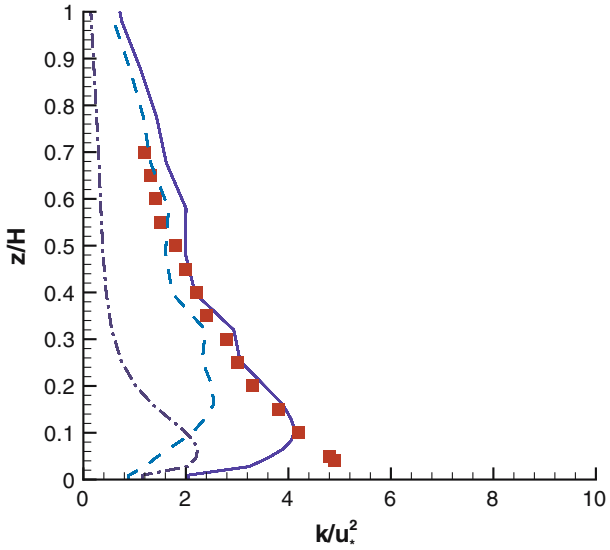

Fig. 2 Vertical profile of fluid turbulent kinetic energy. Continuous lines–our simulation: broken line–resolved; dashed-dotted–sub-grid; solid line–total; squares–measurements of Fackrell and Robins (1982)

The vertical profile of the horizontal mass flux at the end of the saltating bed is shown on Fig. 3. The computed mass flux profile is in good agreement with the experimental results. Nalpanis et al. (1993) only presented the mass flux profile at 6 m and stated that there is no difference between the profiles at 4 and 6 m. On Fig. 3 the computed profile at 4 m is presented illustrating no changes for the computed profiles between $x = 4$ m and $x = 6$ m. Even though the turbulence is practically not resolved near the wall, the mass flux profile of the saltating sand grains is properly simulated. However, the mass flux profiles are sensitive to the determination of the normalization quantities (the mass flux at the sand bed and the boundary-layer depth). When saltation is established, the mass flux at the bed is extremely difficult to measure and the boundary-layer depth deviates from the depth of a boundary layer with no particles.

Figure 4 shows the computed time evolution of the mean rise height, $h_{\max}$, compared to the time-averaged measured value. The time-averaged mean rise height obtained by our simulations is presented in Table 2. Our results are in good agreement with the experimental results of Nalpanis et al. (1993) as well as with normalized predictions of Owen (1964). The mean rise height obtained by our simulations decreases in time because there are more and more sand particles making small hops near the sand bed that are taken into account in the mean.

The time evolution of the mean impact velocity, v_{imp}, is presented in Fig. 5 and the corresponding time average is shown in Table 2. Nalpanis et al. (1993) found that the time-averaged impact speed is 1.6–2 times greater than the time-averaged ejection speed because the drag force increases the velocity of particles. They also measured that the time-averaged ejection speed varies between $3.5u_*$ and $4.4u_*$. From particle trajectory photographs Willetts and Rice (1985) measured a time-averaged impact velocity of $9u_*$, while White and Schulz (1977) obtained $|v_{imp}| \sim 4u_*$. Except for the experimental results of Willetts and Rice (1985) that are relatively high, the results

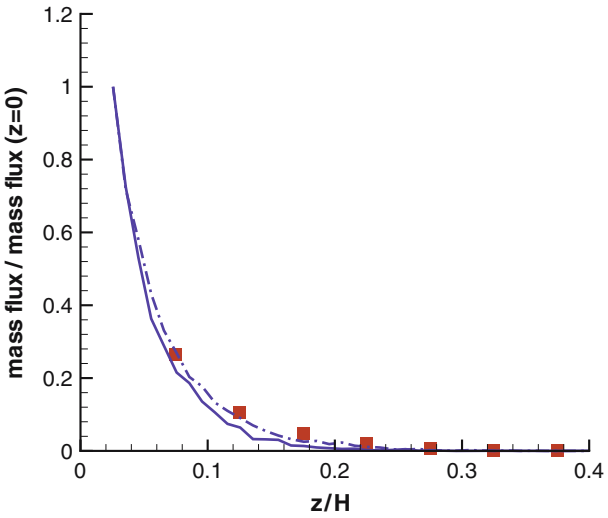

Fig. 3 Vertical profile of sand particle mass flux at 4 m and 6 m. Solid line—our simulation at $x = 6$ m; dashed line—our simulation at $x = 4$ m; squares—experimental results of Nalpanis et al. (1993) at $x = 6$ m

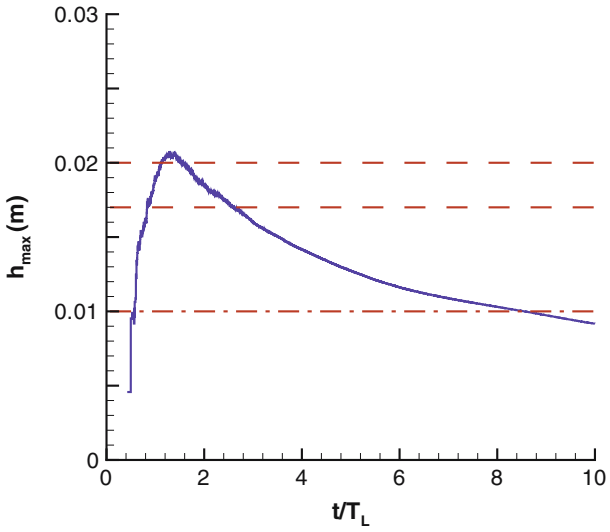

Fig. 4 Time evolution of the mean rise height. Solid line—our simulation; dashed—time averaged value measured by Nalpanis et al. (1993); dashed-dotted—time averaged value predicted by Owen (1964)

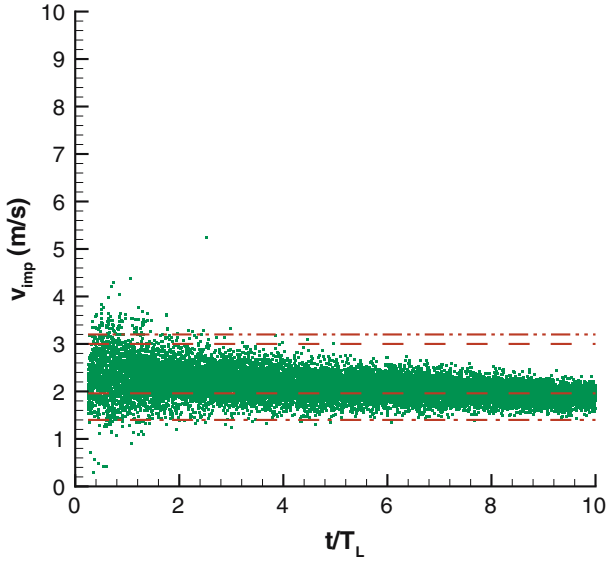

Fig. 5 Time evolution of the mean impact velocity. Squares—our simulation; dashed—time-averaged value measured by Nalpanis et al. (1993); chain-time- averaged value measured by White and Schulz (1977); dashed-dotted—time averaged value measured by Willetts and Rice (1985)

Table 2 Time-averaged values of the mean rise height and the impact velocity

Our simulations	Nalpanis et al. (1993)	Owen (1964)
$h_{\max} = 0.013\,\mathrm{m}$	$h_{\max} = 0.02 - 0.017\,\mathrm{m}$	$h_{\max} = 0.01\,\mathrm{m}$
Our simulations	Nalpanis et al. (1993)	White and Schulz (1977)
$v_{\mathrm{imp}} = 2.1\,\mathrm{m\,s^{-1}}$	$v_{\mathrm{imp}} = 3 - 1.96\,\mathrm{m\,s^{-1}}$	$v_{\mathrm{imp}} = 1.4\,\mathrm{m\,s^{-1}}$
	Willetts and Rice (1985)	
	$v_{\mathrm{imp}} = 3.15\,\mathrm{m\,s^{-1}}$	

of our simulations are within the boundary values measured by Nalpanis et al. (1993) and in good agreement with the results found by White and Schulz (1977).

8.2 Sand and PVC particles in modified saltation, Tanière et al. (1997)

The dispersion of PVC and sand particles in saltation and modified saltation in a turbulent boundary layer over a flat bed without particles is studied in this experiment. The main characteristics of the flow and particles are given in Tables 3 and 4, respectively. Particles are introduced into the flow by means of an upward moving piston that is driven by an electric motor. In the numerical simulation, particles are injected into the flow in accordance with the experimental conditions. Each injected particle has a vertical velocity that is equal to the velocity of the upward moving piston. The size is determined from sampling according to the size distribution given by the experiments. Profiles of wind speed, fluid velocity fluctuations, particle velocities and mass flux profiles are measured at the end of the domain.

In this test case, an analogous boundary-layer flow is simulated, and similarity is obtained by conserving the Reynolds number $Re = HU_e/\nu$. For the Stokes numbers (St_η and St_L) and the gravity parameter (γ), only the regimes are preserved and not the exact values. Details concerning the similarity may be found in Vinkovic (2005). A grid with $330 \times 32 \times 32$ points is used. The grid spacing in the longitudinal and transverse direction is $\Delta x/H = \Delta y/H = 0.08$. In the vertical direction, the average grid is $\Delta z_{\mathrm{mean}}/H = 0.08$ and the first grid is at $\Delta z_{\mathrm{min}}/H = 0.0025$.

Table 3 Flow characteristics, Tanière et al. (1997)

Boundary-layer height	$H = 0.07\,\mathrm{m}$
External velocity	$U_e = 10.6\,\mathrm{m\,s^{-1}}$
Friction velocity	$u_* = 0.40\,\mathrm{m\,s^{-1}}$

Table 4 Particle characteristics, Tanière et al. (1997)

	Sand	PVC
Mean particle diameter (m)	$d_p = 60 \times 10^{-6}$	$d_p = 130 \times 10^{-6}$
Diameter standard deviation (m)	18×10^{-6}	46.2×10^{-6}
Particle density (kg m^{-3})	$\rho_p = 2500$	$\rho_p = 1430$
Stokes number	$St_L = 0.41$	$St_L = 0.87$
	$St_\eta = 27.9$	$St_\eta = 58.5$
Gravity parameter	$\gamma = 0.64$	$\gamma = 1.33$
Volume fraction	$\Phi_p \sim 10^{-4}$	$\Phi_p \sim 10^{-4}$

Figures 6–9 show predicted profiles of mean fluid velocity U, turbulent kinetic energy k, streamwise and vertical velocity fluctuations (u'^2 and w'^2), respectively, compared to the experimental data. The turbulent kinetic energy profile is compared to the normalized profile measured by Fackrell and Robins (1982), because the corresponding profile was not published by Tanière et al. (1997). The LES resulted in a fairly accurate prediction of the mean velocity (Fig. 6). After the addition of the subgrid part of the turbulent kinetic energy (Xie et al. 2004), good agreement is achieved between the simulated and the experimental profiles of the turbulent kinetic energy (Fig. 7). The turbulent kinetic energy has a large-scale and a SGS contribution. For both cases the SGS contribution is around 20% at least, for $z/H \geq 0.2$, and increases rapidly as we approach the wall to values higher than 50% of the total turbulent kinetic energy. The stochastic model is thus an important contribution to the total turbulent kinetic energy and provides a component as large as the one obtained directly by the LES. Anisotropy causes discrepancies in the near wall region that increase if a lower resolution is used (Xie et al. 2004). This is the case here, as the resolution is lower for the test of Nalpanis et al. (1993) than for the test of Tanière et al. (1997). Yet, the total turbulent kinetic energy is recovered by addition of the SGS part.

The streamwise component of velocity fluctuations is under-evaluated by our simulations (Fig. 8). However, when compared to the experimental results of Fackrell and Robins (1982), it seems that the streamwise velocity fluctuation measured by Tanière et al. (1997) is slightly overestimated. In Tanière et al. (1997) measurements of flow characteristics without particles were performed by a hot wire probe.

Close to the wall, the volume fraction of sand or PVC particles is $\Phi_p \sim 10^{-4}$. Nevertheless, there are no obvious effects of the two-way coupling on the mean fluid velocity profile or on the turbulent kinetic energy.

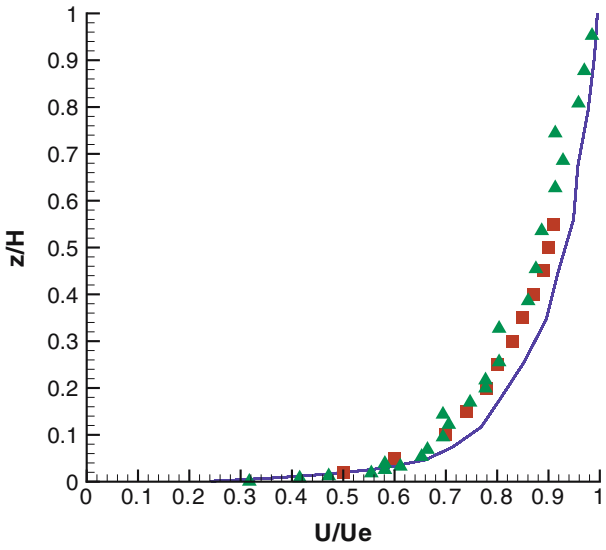

Fig. 6 Vertical profile of streamwise mean fluid velocity. Continuous line—our simulation; squares-measurements of Fackrell and Robins (1982); triangles—measurements of Tanière et al. (1997)

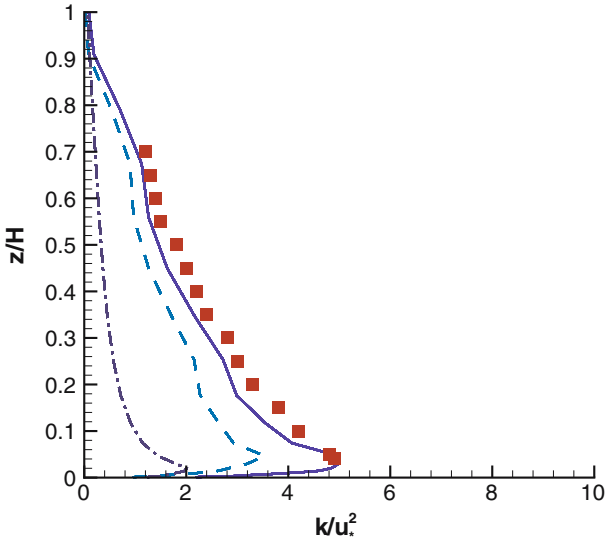

Fig. 7 Vertical profile of fluid turbulent kinetic energy. Continuous lines—our simulation: broken line—resolved; dashed-dotted—sub-grid; solid line—total; squares—measurements of Fackrell and Robins (1982)

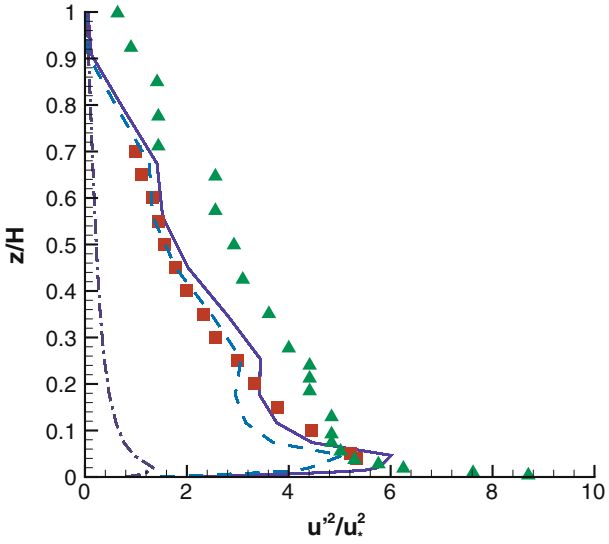

Fig. 8 Vertical profile of fluid streamwise velocity fluctuation. Continuous lines—our simulation: broken line—resolved; dashed-dotted—sub-grid; solid line—total; triangles—measurements of Tanière et al. (1997); squares—measurements of Fackrell and Robins (1982)

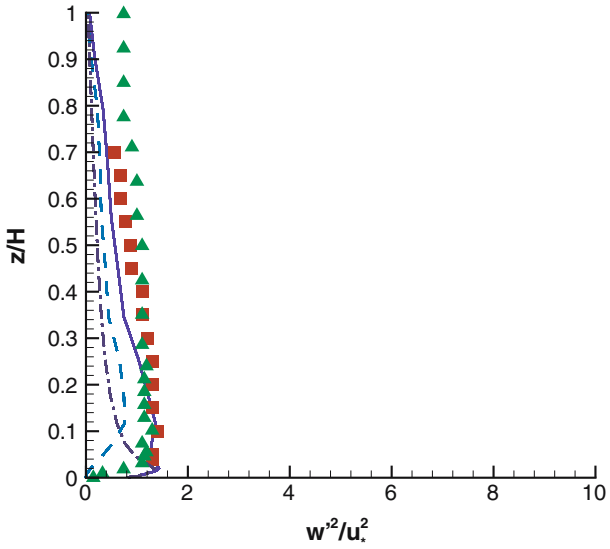

Fig. 9 Vertical profile of fluid vertical velocity fluctuation. Continuous line-our simulation: broken line—resolved; dashed-dotted—sub-grid; solid line—total; triangles—measurements of Tanière et al. (1997); squares—measurements of Fackrell and Robins (1982)

The vertical profile of mass flux at $x = 5.06\,\mathrm{m}$ is shown in Fig. 10. The computed mass flux profile is in good agreement with the experimental results, both for PVC and for sand particles. As expected, the particle mass flux decreases with increasing distance from the wall, exhibiting an almost exponential shape. Sand particles, which are lighter, reach higher elevations than PVC particles, and their mass flux profile is closer to being homogeneous. Near the wall, the PVC mass flux is larger due to gravity.

In Fig. 11, the dimensionless mean velocity profile of sand and PVC ($v_{p,1}$) is displayed and compared with the experimental results. Away from the wall the mean velocity of both types of particles is slightly overestimated. This is due to the overestimation in the mean fluid velocity away from the wall (Fig. 6). In our simulations the velocity of sand and PVC particles is very close to the mean velocity profile of the carrier fluid. Tanière et al. (1997) found that the mean particle velocity is slightly lower than that of the fluid except very close to the wall. Due to particle-wall interactions the mean velocity of the dispersed phase reaches a non-zero value at the wall.

Figures 12 and 13 illustrate the vertical profiles of the streamwise and vertical velocity fluctuations for both PVC and sand ($v'_{p,1}$ and $v'_{p,3}$). Concerning the streamwise velocity fluctuations, good agreement is achieved near the wall. The noisy character of the data away from the wall is due to an insufficient number of particles in that region of the flow. Even though 250,000 particles are tracked at each timestep, outside the saltation layer few particles exist. In this region of the flow, accurate statistics are hardly achieved no matter how many particles are tracked. The vertical velocity fluctuations obtained by the present simulation are slightly overestimated compared to the experimental results near the wall, and may be due to the rebound condition. The computed vertical particle turbulent intensities are larger than those of the fluid. Particle velocity fluctuations are not only due to fluid turbulence but also to inertia and

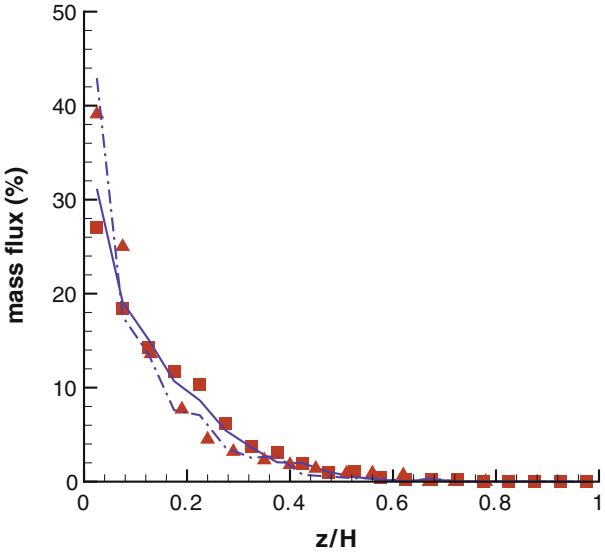

Fig. 10 Vertical profile of mass flux for sand and PVC particles at $x = 5.06$ m. Solid line—our simulation for sand; dashed-dotted—our simulation for PVC; squares—experimental results of Tanière et al. (1997) for sand; triangles—experimental results of Tanière et al. (1997) for PVC

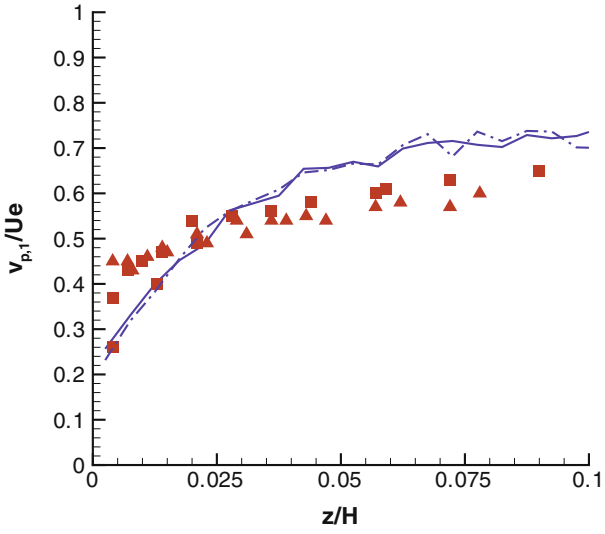

Fig. 11 Vertical profile of sand and PVC mean velocity $v_{p,1}$ at $x = 5.06$ m. Solid line—our simulation for sand; dashed-dotted—our simulation for PVC; squares—experimental results of Tanière et al. (1997) for sand; triangles—experimental results of Tanière et al. (1997) for PVC

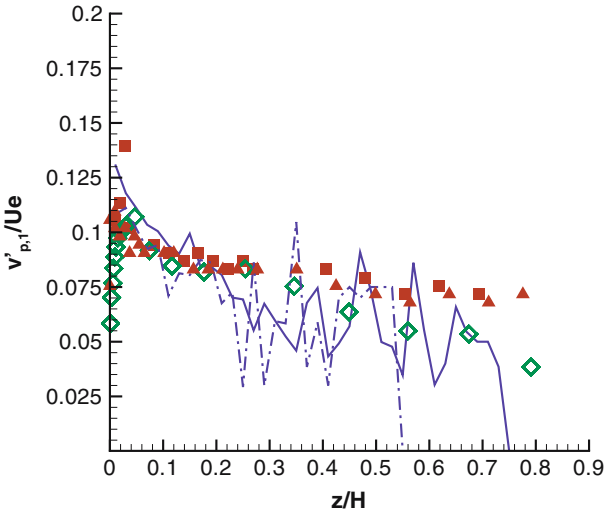

Fig. 12 Vertical profile of sand and PVC longitudinal fluctuating velocity $v'_{p,1}$, at $x = 5.06$ m. Solid line—our simulation for sand; dashed-dotted—our simulation for PVC; diamonds—our simulation for fluid; squares—experimental results of Tanière et al. (1997) for sand; triangles—experimental results of Tanière et al. (1997) for PVC

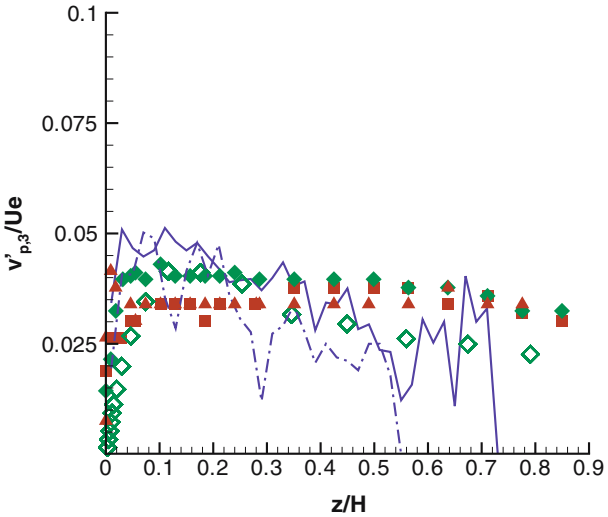

Fig. 13 Vertical profile of sand and PVC vertical fluctuating velocity $v'_{p,3}$, at $x = 5.06$ m. Solid line—our simulation for sand; dashed-dotted—our simulation for PVC; diamonds—our simulation for fluid; squares—experimental results of Tanière et al. (1997) for sand; triangles—experimental results of Tanière et al. (1997) for PVC; full diamonds—experimental results of Tanière et al. (1997) for fluid

gravity effects. The present results indicate that, in the vertical direction, the effects of gravity and inertia may prevail over the turbulence effect in the case of saltation. For both components of the fluctuating velocity no significant difference can be observed between the sand and PVC particles.

8.3 Some additional results

With the approach adopted in this study, second- or higher-order statistics on concentration or particle velocities are obtained directly from the computed results with no additional computational costs or modelling assumptions. To illustrate this, vertical profiles of root-mean-square concentration, skewness and flatness coefficients will be shown, obtained from the numerical simulation of the case of Nalpanis et al. (1993), Sect. 8.1. They are not compared with experimental results because of the lack of data. It should be noted that, since the stochastic SGS model for particle transport is a one-particle model, spatial correlations among different particles are neglected.

The relative root-mean-square concentration profiles $c'(z)/\bar{C}_{\max}$, at two positions of the sand bed ($x = 4$ m and $x = 6$ m) are shown in Fig. 14. Except close to the bed, both profiles exhibit similar shapes. As the distance x increases, close to the bed, $c'/\bar{C}_{\max}$ increases, and could be explained by the increase in the number of particles impacting the sand bed and ejecting particles. As x increases, saltation becomes an established process.

Figures 15 and 16 represent the skewness and the flatness coefficients given by:

$$S = \frac{\overline{c'^3}}{\left(\overline{c'^2}\right)^{3/2}}, \tag{38a}$$

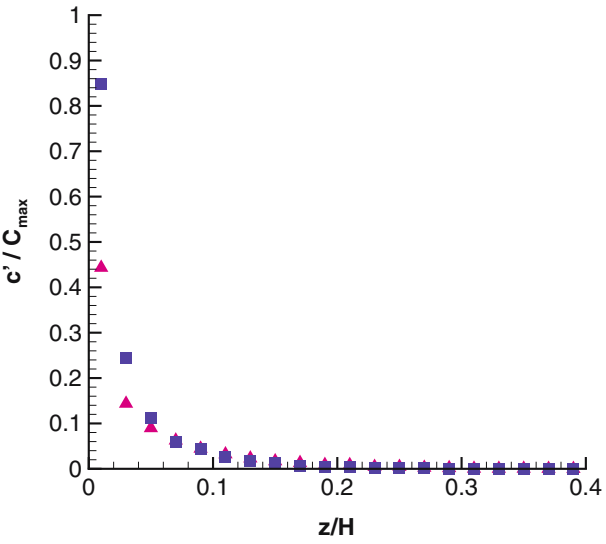

Fig. 14 Vertical profile of sand particle root-mean square concentration at 4 m and 6 m. Squares—our simulation at $x = 6$ m; triangles—our simulation at $x = 4$ m

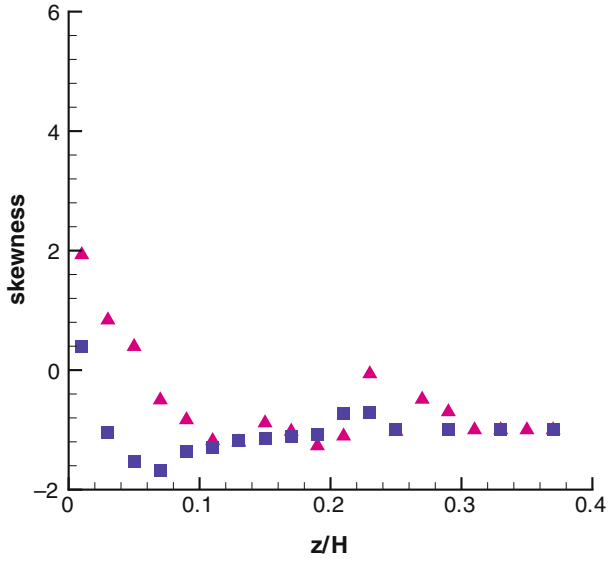

Fig. 15 Vertical profile of sand particle skewness coefficient at 4 m and 6 m. Squares—our simulation at $x = 6$ m; triangles—our simulation at $x = 4$ m

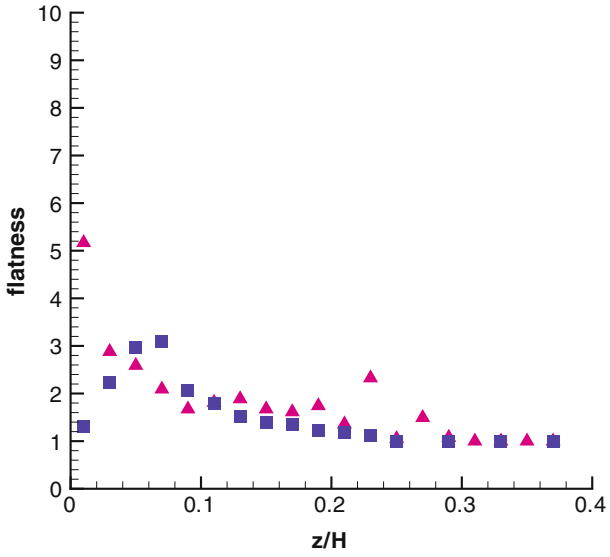

Fig. 16 Vertical profile of sand particle flatness coefficient at 4 m and 6 m. Squares—our simulation at $x = 6$ m; triangles—our simulation at $x = 4$ m

$$K = \frac{\overline{c'^4}}{\left(\overline{c'^2}\right)^2}, \tag{38b}$$

respectively. Near the sand bed, values of the skewness coefficient decrease from around 1, reaching a stable value around −1, from $z/H \geq 0.1$. The flatness coefficient also reaches a stable value of 1, beginning from $z/H = 0.2$. For both coefficients, the values taken are completely different from the corresponding values for Gaussian variables ($S = 0$ and $K = 3$). The flatness coefficient plotted against the skewness coefficient is represented in Fig. 17. The profiles have a parabolic form, a fact previously reported by Mole and Clarke (1995) and Chatwin and Sullivan (1990) for scalar dispersion in turbulent shear flows. After mathematical analysis, the authors found that, for any type of probability density function of the concentration, the flatness versus the skewness coefficient satisfies $K \geq S^2 + 1$. The inequality is satisfied when molecular diffusion is neglected.

9 Conclusions

A LES coupled with a Lagrangian stochastic model has been applied to the study of solid particle dispersion in a turbulent boundary layer. Solid particles are tracked in a Lagrangian way. The velocity of the fluid particle along the solid particle trajectory is considered to have a large-scale part and a small-scale part given by a modified three-dimensional Langevin model using the filtered SGS statistics. An appropriate Lagrangian correlation time scale is considered in order to include the influences of gravity and inertia. The use of a subgrid model for the displacement of particles becomes essential when LES is applied to atmospheric flows, where grids ranging

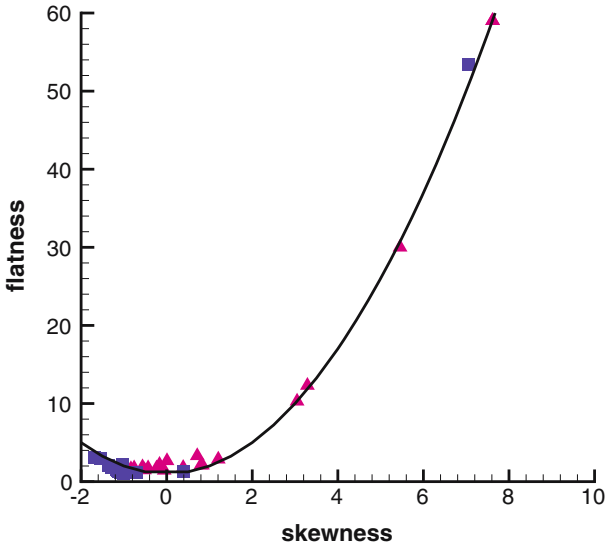

Fig. 17 Flatness coefficient, K, versus the skewness coefficient, S, at 4 m and 6 m Squares—our simulation at $x = 6$ m; triangles—our simulation at $x = 4$ m; solid line — $K = S^2 + 1$

from 10 to 50 meters for the convective boundary layer and attaining 100 meters to a few kilometers in simulations of mesoscale phenomena, are used. Two-way coupling, inter-particle collisions and grain-bed interactions are also taken into account. A stochastic approach is adopted for the splash function that characterizes the grain-bed interactions.

The entire modelling is then applied to the wind-tunnel experiments of Nalpanis et al. (1993) and of Tanière et al. (1997). Good agreement is achieved for mass flux profiles and statistics on grain-bed impact. In the second test case, sand and PVC particles are dispersed over a flat bed without particles. This case was simulated without the splash function and with simple symmetry conditions for particle rebound. This way, an additional validation without the influence of the splash model is achieved. Vertical profiles of mass flux and mean particle velocity are in agreement with the experimental results. Few particles exist outside the saltation layer, and so, in this region of the flow, accurate second-order statistics are difficult to obtain.

Because of Lagrangian particle tracking and the subgrid stochastic model, mass fluxes and second- or higher-order statistics on concentration or particle velocities can be obtained directly from the computed results with no additional computational costs or modelling assumptions, as long as there are enough particles in the flow. However, since the stochastic SGS model for particle transport is a one-particle model, spatial correlations among different particles are neglected. Further developments will tend to introduce thermal effects, the impact of humidity on grain-bed interactions as well as on particle dispersion, and electrostatic forces that may take place between dust particles in high concentration clouds of dust storms. The main objective is also to apply the developed tools to real conditions and validate the coupling with in-situ measurements. This should ultimately provide a physically sound and efficient tool for the computation of atmospheric dust and sand dispersion.

References

Aguirre C, Guo Y, Ayrault M (2004) Dispersion of solid saltating particles in a turbulent flow. CR, Mec 332: 627–632

Anderson RS (1986) Sediment transport by wind: saltation, erosion and ripples. PhD thesis, University of Washington

Anderson RS, Haff PK (1991) Wind Modification and bed response during saltation of sand in air. Acta Mech Suppl 1:21–51

Bagnold RA (1941) The physics of blown sand and desert dunes, Chapman and Hall, 265 pp

Batt RG, Petach MP Peabody II SA, Batt RR (1999) Boundary layer entrainment of sand-sized particles at high speed. J Fluid Mech 392:335–360

Chatwin PC, Sullivan PJ (1990) A simple and unifying physical interpretation of scalar fluctuation measurements from many turbulent shear flows. J Fluid 'Mech 212:533–556

Clift R, Grace JR, Weber ME (1978), Bubbles, drops and particles, Academic Press, New York, 380 pp

Csanady GT (1963) Turbulent diffusion of heavy particles in the atmosphere. J Atmos Sci 20:201–208

Deardorff JW (1970) A Numerical study of three-dimensional turbulent channel flow at large reynolds numbers. J Fluid Mech 41:453–480

Deardorff JW (1980) Stratocumulus-capped mixed layer derived from a three-dimensional model. Boundary-Layer Meteorol 18:495–527

Doorschot JJ, Lehning M (2002) Equilibrium saltation: mass fluxes, aerodynamic entrainment, and dependence on grain properties. Boundary-Layer Meteorol 104:111–130

Dudhia J (1993) A nonhydrostatic version of the penn state NCAR mesoscale model: validation tests and simulation of an atlantic cyclone and cold front. Mon Wea Rev 121:1493–1513

Elghobashi S (1994) On predicting particle-laden turbulent flows. Appl Sci Res 52:309–329

Fackrell JE, Robins AG (1982) Concentration fluctuations and fluxes in plumes from point sources in a turbulent boundary layer. J Fluid Mech 117:1–26
Fohanno S, Oesterlé B (2000) Analysis of the effect of collisions on the gravitational motion of large particles in a vertical duct. Int J Multiphase Flow 26:267–292
Foucaut JM, Stanislas M (1997) Experimental study of saltating particle trajectories. Exp Fluids 22:321–326
Germano M, Piomelli U, Moin P, Cabot WH (1991) A dynamic subgrid-scale viscosity model. Phys Fluids 3:1760–1765
Hanna SR (1981) Lagrangian and eulerian time-scale relations in the daytime boundary layer. J Appl Meteorol 20:242–249
Johnson KW, Bauer GA, Riccardi J, Droegemeier KK, Xue M (1994) Distributed processing of a regional prediction model. Month Wea Rev 122:2558–2572
Kaftori D, Hestroni G, Banerjee S (1995) Particle behaviour in the turbulent boundary layer. I. motion, deposition, and entrainment. Phys Fluids 7:1095–1106
Klemp JB, Wilhelmson R (1978) The simulation of three- dimensional convective storm dynamics. J Atmos Sci 35:1070–1096
Lafore JP, Stein J, Asencio N, Bougeault P, Ducrocq V, Duron J, Fischer C, Héreil P, Mascart P, Masson V, Pinty JP, Redelsperger JL, Richard E, Vilà-Guerau de Arellano J (1998) The Meso-NH atmospheric simulation system. Part I: adiabatic formulation and control simulations. Ann Geophysicae 16:90–109
Lilly DK (1992) A proposed modification of the germano subgrid-scale closure method. Phys Fluids 4:633–635
Lu H, Shao Y (1999) A new model for dust emission by saltation bombardment. J Geophys Res 104:16827–16842
Marticorena B, Bergametti G (1995) Modelling the atmospheric dust cycle: 1. design of a soil-derived dust emission scheme. J Geophys Res 100:16415–16430
Marticorena B, Bergametti G, Aumont B (1997) Modelling the atmospheric dust cycle: 2. simulation of sahara dust sources. J Geophys Res 102:4387–4404
McEwan IK, Willetts BB (1991) Numerical model of the saltation cloud. Acta Mech Suppl 1:53–66
McEwan IK, Willetts BB, Rice MA (1992) The grain/bed collision in sand transport by wind. Sedimentology 39:971–981
McKenna Neuman C (2003) Effects of temperature and humidity upon the entrainment of sedimentary particles by wind. Boundary-Layer Meteorol 108:61–89
Meneveau C, Katz J (2000) Scale-invariance and turbulence model for large-eddy simulation. Annu Rev Fluid Mech 32:1–32
Mitha S, Tran MQ, Werner BT, Haff PK (1986) The Grain-Bed Impact in Aeolian Saltation', Acta Mechanica 63:267–278
Mole N, Clarke ED (1995) Relationships between higher moments of concentration and of dose in turbulent dispersion. Boundary-Layer Meteorol 73:35–52
Nalpanis P, Hunt JCR, Barrett CF (1993) Saltating particles over flat beds. J Fluid Mech 251:661–685
Owen PR (1964) Saltation of uniform grains in air. J Fluid Mech 20:225–242
Pan Y, Banerjee S (1996) Numerical simulation of particle interactions with wall turbulence. Phys Fluids 8:2733–2755
Porahmadi F, Humphrey JAC (1983) Modeling solid turbulent flows. Physico Chem Hydrodyn 191–219
Pope BS (1985) PDF methods for turbulent reactive Flows. Prog Energy Combust Sci 11:119–192
Pozorski J, Apte SV, Raman V (2004) Filtered particle tracking for dispersed two-phase turbulent flows. Center for turbulence research, proceedings of the summer program, 329–340
Pozorski J, Minier J-P (1998) On the lagrangian turbulent dispersion models based on the langevin equation. Int J Multiphase Flow 24:913–945
Reynolds AM (1999) A lagrangian stochastic model for heavy particle deposition. J Colloid Int Sci 215:85–91
Reynolds AM (2000) On the formulation of lagrangian stochastic models for heavy-particle trajectories. J Colloid Int Sci 232:260–268
Reynolds AM, Cohen JE (2002) Stochastic simulation of heavy-particle trajectories in turbulent flows. Phys Fluids 14:342–351
Rice MA, Willetts BB, McEwan IK (1996) Observations of collisions of saltating grains with granular bed from high-speed cine-film. Sedimentology 43:21–31
Rodgers CB, Eaton JK (1990) The behaviour of solid particles in a vertical turbulent boundary layer. Int J Multiphase Flow 16:819–834
Sawford BL, Guest FM (1991) Lagrangian statistical simulation of the turbulent motion of heavy particles. Boundary-Layer Meteorol 54:147–166

Shao Y (1995) The fractional ornstein-uhlenbeck process as a representation on the entrainment of dust by wind. Physica D 83:461–477
Shao Y (2000) Physics and modelling of wind erosion, Kluwer Academic Publishers Dordrecht, p 393
Shao Y (2005) A similarity theory for saltation and application to aeolian mass flux. Boundary-Layer Meteorol 115:319–338
Shao Y, Raupach MR, Leys JF (1996) A model for predicting aeolian sand drift and dust entrainment on scales from paddock to region. Aust J Soil Res 34:309–342
Shao Y, Leslie LM (1997) Wind erosion prediction over the australian continent. J Geophys Res 102:30091–30105
Shao Y, Li A (1999) Numerical modeling of saltation in the atmospheric surface layer. Boundary-Layer Meteorol 91:199–225
Shao Y, Lu H (2000) A simple expression for wind erosion threshold friction velocity. J Geophys Res 105:22437–22443
Sommerfeld M (2001) Validation of a stochastic lagrangian modeling approach for inter-particle collisions in homogeneous isotropic turbulence. Int J Multiphase Flow 27:1829–1858
Sorensen M (1991) An analytic model of wind-blown sand transport. Acta Mech Suppl 1:67–81
Tanaka T, Tsuji Y (1991) Numerical simulation of gas-solid two-phase flow in a vertical pipe: on the effect of inter-particle collision. Gas-Solid Flows FED ASME 121:123–128
Tanière A, Oesterlé B, Monnier JC (1997) On the behaviour of solid particles in a horizontal boundary layer with turbulence and saltation. Exp in Fluids 23:463–471
van Dop H, Nieuwstadt FTM, Hunt JCR (1986) Random walk models for particle displacement in inhomogeneous unsteady turbulent Flows. Phys Fluids 28:1639–1653
Vinkovic I (2005) Dispersion et mélange turbulents de particules solides et de gouttelettes par une simulation des grandes échelles et une modélisation stochastique lagrangienne. PhD thesis, Ecole Centrale de Lyon
Vinkovic I, Aguirre C, Simoëns S, Gence JN (2005a) Coupling of a subgrid lagrangian stochastic model with large-eddy simulation. CR Mecanique 333:325–330
Vinkovic I, Aguirre C, Simoëns S (2005b) Large-eddy simulation and lagrangian stochastic modeling of passive scalar dispersion in a turbulent boundary layer. J Turbulence in press.
Wang Q, Squires KD (1996) Large eddy simulation of particle-laden turbulent channel flow. Phys Fluids 8(5):1207–1223
Wang LP, Stock DE (1993) Dispersion of Heavy Particles by Turbulent Motion. J Atmos Sci 50:1897–1913
White BR, Schulz JC (1977) Magnus effect in saltation. J Fluid Mech 81:497–512
Willetts BB, Rice MA (1985) Inter-saltation collisions. proceedings of the international workshop on the physics of blown sand, Aarhus University, Denmark 8:83–100
Willetts BB, Rice MA (1986) Collisions in aeolian saltation. Acta Mechanica 63:255–265
Willetts BB, McEwan IK, Rice MA (1991) Initiation of the motion of quartz sand grains. Acta Mechanica Suppl 1:123–134
Xie Z, Hayden P, Voke PR, Robins AG (2004) Large-eddy simulation of dispersion: comparison between elevated and ground-level sources. J Turbulence 5:1–15
Xue M, Droegemeier KK, Wong V (2000) The advanced regional prediction system (ARPS)-A multi-scale nonhydrostatic atmospheric simulation and prediction model. Part I: model dynamics and verification. Meteorol Atmos Phys 75:161–193
Xue M, Droegemeier KK, Wong V, Shapiro A, Brewster K, Carr F, Weber D, Liu Y, Wang D (2001) The Advanced regional prediction system (ARPS)-A multi-scale nonhydrostatic atmospheric simulation and prediction tool. Part II: model physics and applications. Meteorol Atmos Phys 76:143–165
Yamamoto Y, Potthoff M, Tanaka T, Kashijima T, Tsuji Y (2001) Large-eddy simulation of turbulent gas-particle flow in a vertical channel: effects of considering inter-particle collisions. J Fluid Mech 442:303–334
Yeung PK (2001) Lagrangian characteristics of turbulence and scalar transport in direct numerical simulations. J Fluid Mech 427:241–274
Zhuang Y, Wilson JD, Lozowski EP (1989) A trajectory-simulation model for heavy particle motion in turbulent flow. Transactions of the ASME, J Fluid Eng 111:492–494